energies

MDPI

Article

Maximum Safety Regenerative Power Tracking for DC Traction Power Systems

Guifu Du [1], Dongliang Zhang [1], Guoxin Li [1,*], Yihua Hu [2], Yang Liu [2], Chonglin Wang [1] and Jianhua Liu [1]

[1] School of Electrical and Power Engineering, China University of Mining and Technology, Xuzhou 221008, China; cumt_dgf@126.com (G.D.); zdl@cumt.edu.cn (D.Z.); chlwang@cumt.edu.cn (C.W.); ljh5605@126.com (J.L.)

[2] Department of Electrical Engineering & Electronic, University of Liverpool, Liverpool L69 3BX, UK; Y.Hu35@liverpool.ac.uk (Y.H.); Yang.Liu@liverpool.ac.uk (Y.L.)

* Correspondence: lee_guoxin@126.com; Tel.: +86-516-8388-5605

Academic Editor: Paul Stewart

Received: 25 December 2016; Accepted: 12 February 2017; Published: 17 February 2017

Abstract: Direct current (DC) traction power systems are widely used in metro transport systems, with running rails usually being used as return conductors. When traction current flows through the running rails, a potential voltage known as "rail potential" is generated between the rails and ground. Currently, abnormal rises of rail potential exist in many railway lines during the operation of railway systems. Excessively high rail potentials pose a threat to human life and to devices connected to the rails. In this paper, the effect of regenerative power distribution on rail potential is analyzed. Maximum safety regenerative power tracking is proposed for the control of maximum absolute rail potential and energy consumption during the operation of DC traction power systems. The dwell time of multiple trains at each station and the trigger voltage of the regenerative energy absorbing device (READ) are optimized based on an improved particle swarm optimization (PSO) algorithm to manage the distribution of regenerative power. In this way, the maximum absolute rail potential and energy consumption of DC traction power systems can be reduced. The operation data of Guangzhou Metro Line 2 are used in the simulations, and the results show that the scheme can reduce the maximum absolute rail potential and energy consumption effectively and guarantee the safety in energy saving of DC traction power systems.

Keywords: direct current (DC) traction power systems; rail potential; regenerative energy distribution; operation optimization

1. Introduction

Direct current (DC) traction power system is widely used in metro transport systems, with running rails usually being used as return conductors. Due to the longitudinal resistance of the running rails and the ungrounded scheme of the system, a potential will exist between the running rails and the ground when a traction current flows back to the traction substation, which is known as rail potential. Since the running rails cannot be completely insulated from the ground, some of the return current will leak from the running rails into the surrounding ground, which is called stray current. Currently, abnormal rail potential rises and stray currents have become a serious safety hazard during the operation of DC traction power systems [1,2]. An excessive rail potential poses a risk to human life and to the devices connected to the rails, and the stray current will increase the electrochemical corrosion of the reinforcing bars and buried metal pipelines [3,4]. In order to guarantee human safety and normal operation of equipment, regulations controlling the rail potential in DC traction power systems should be designed [5,6]. According to relevant standards [7,8], the maximum

absolute rail potential in the line should not exceed 90 V. Overvoltage protection devices (OVPDs) are set at the station to connect the rail to the ground when the rail potential exceeds the standard limits [9]. In this situation, the leakage of return current will increase, and the stray current hazard becomes more serious. Therefore, the abnormal rise of rail potential cannot be completely controlled by OVPDs.

Rail potential is highly affected by the power distribution of DC traction power systems [10,11]. For the electrical connectivity of the catenaries and running rails in the whole line, an abnormal rise of rail potential caused by the regenerative power transferring over power sections is obvious [11]. As demonstrated in Figure 1a, the regenerative energy fed back to the catenary by the braking trains P_{reg} can be absorbed by the accelerating trains. When the catenary voltage at regenerative energy absorbing device (READ) exceeds its trigger voltage, the READ is activated to absorb the remaining regenerative energy. The regenerative power absorbed by other accelerating trains may increase the utilization of regenerative power, but the power transferring with a long distance leads to the increase of power loss in traction network and the abnormal rise of rail potential. As shown in Figure 1b, there are no accelerating trains in the line to absorb the regenerative power, then the regenerative power is absorbed by READ at the power section with a short distance, and the rail potential is low. In many railway lines, the energy absorbed by READ is wasted by heating resistors, which becomes the energy consumption of the system. In this paper, the maximum safety regenerative power tracking is proposed to realize the control of maximum absolute rail potential and energy consumption in the system. The dwell time at each station and trigger voltage of each READ are optimized to manage the regenerative power distribution.

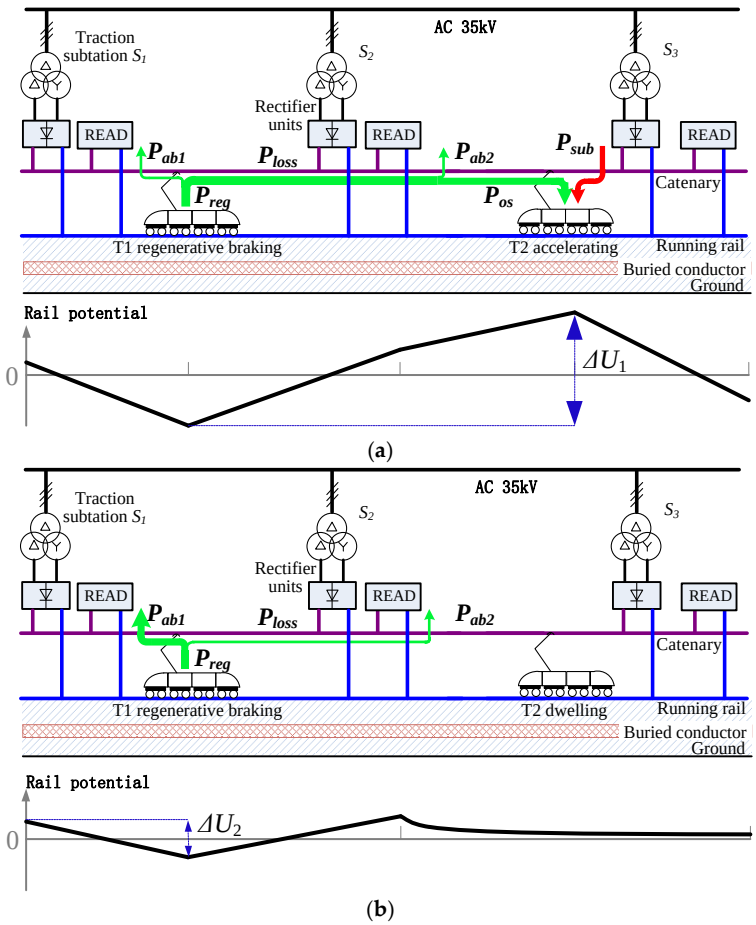

Figure 1. Diagram of regenerative power distribution and rail potential. (**a**) Regenerative energy transferring over sections with a long distance; (**b**) Regenerative energy absorbed with a short distance.

In recent years, rail potential distribution and control methods have been studied. The results of [1] and [2] show that, increasing the power voltage of the system, shorting the distance between traction substations, and reducing the longitudinal resistance of running rails can effectively decrease the rail potential. Different grounding schemes have an impact on the distribution of rail potential, such as solid grounded, diode grounded, and ungrounded [12]. In addition, the running modes of trains during the operation of railway systems will affect the rail potential and stray current [9,13]. These studies are based on simulation models with single or double power sections, and the effect of power distribution on rail potential when multiple trains run in multiple sections is ignored. Cross-track regeneration supply and over zone feeding have an impact on rail potential and stray current [10,14]. Du proposed a power distribution model to analyze the abnormal rise of rail potential based on the power distribution of the system [11]. Results of simulations and field tests show that rail potential is highly affected by the power distribution. Although the existing studies clarify the abnormal rise of rail potential caused by power distribution, control methods with power distribution management have not been studied.

Regenerative braking is the main braking method of the trains in DC traction power systems. When the train uses regenerative braking, the regenerative energy will be fed back to the catenary. The regenerative energy in the system may be absorbed by accelerating trains, wasted by heating resistors, absorbed by energy storage devices and fed back to the alternating current (AC) side by a regenerative inverter [15]. Currently, the energy storage devices and regenerative inverter are not widely used in the railway lines. Studies on the bidirectional inverter used in DC traction power systems have been carried out, but the electrical protection should be designed [5,16]. Studies have been carried out on the utilization of regenerative energy by energy efficient control of multiple trains. In order to increase the utilization of regenerative energy, optimization models for controlling the trains' running time and schedule has been studied in [17–19]. Relevant studies employ the overlapping time of accelerating trains and braking trains to access the utilization rate of regenerative energy [20]. Yang et al. [21] and Zhao et al. [22] considered the waiting time and the total passenger time in the optimization of train timetable to increase the utilization of regenerative energy. These papers aim to maximize the utilization of regenerative energy, but ignore the electrical safety of the system in the management of regenerative energy.

For the energy saving and abnormal rise of rail potential caused by regenerative power distribution, maximum safety regenerative power tracking is proposed to control the maximum absolute rail potential and system energy consumption. Optimization of multiple trains' dwell time and trigger voltage of READ can change the power distribution in the system. In this paper, an improved particle swarm optimization (PSO) algorithm is proposed to optimize the trains' dwell time and trigger voltage of READ, then the maximum absolute rail potential is reduced effectively and lower energy consumption is achieved. The rest of this paper is organized as follows: in Section 2, the system modeling and the effect of regenerative energy distribution on rail potential are presented. In Section 3, the maximum safety regenerative power tracking is proposed based on an improved PSO algorithm. In Section 4, based on the system parameters and operation data of the Guangzhou Metro Line 2 in China, the effect of control on maximum absolute rail potential and energy consumption with regenerative power management are shown.

2. System Modeling

The DC traction power system mainly consists of rectifier units, catenaries, trains, running rails, buried conductors, READ, etc. In actual lines, the power distribution is more complex than that shown in Figure 1. Catenaries in the up-line and down-line are independent in the interval and connected with each other at the position of traction substation through a DC positive bus. Therefore, the flow path of the regenerative current in DC traction power systems is more complex. In order to obtain the rail potential and energy consumption during the operation of DC traction power systems, the simulation model of the system is designed as shown in Figure 2.

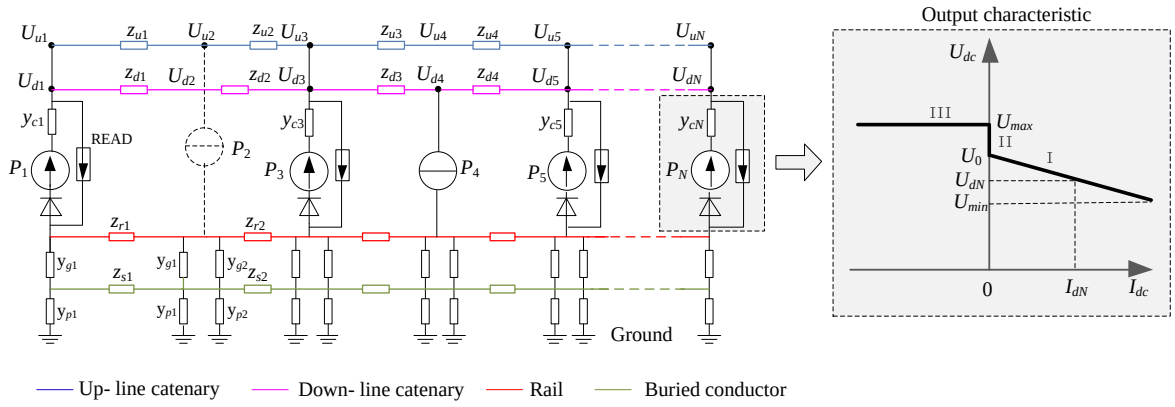

Figure 2. Simulation of DC traction power systems.

In the simulation model of DC traction power systems, a train is equivalent to a power source model in the up-line or down-line, whose power and position are obtained by a train calculation model. Because the train is modelled in the power source, the circuit equations are nonlinear, and the equations need to be solved by an iteration method.

When the train is accelerating, the train power has a positive value, which means that the train obtains power from the catenary. When the train is in regenerative braking mode, the power has a negative value, meaning that the regenerative energy is fed back to the catenary. The rectifier units are power unidirectional with an internal resistance, which are equivalent to a constant voltage source in series connection with an equivalent resistance and a diode. The no-load voltage of the rectifier units is U_0. The READ can be simulated with an adjustable resistance, with a trigger voltage of U_{max}. When voltage of the catenary to the running rail at the position of READ exceeds U_{max}, the READ is activated to absorb the remaining regenerative braking energy to maintain the catenary voltage. Output characteristic of the traction substation with rectifier units and READ is shown in Figure 2. The impedance of the traction network changes with the position of the train. The return circuit is a distributed parameter model, which is always divided into segments of 100–300 m in the simulation, and the segment is equivalent to a lumped parameter model. In the simulation of the whole line, the conductance matrixes of multiple segments will be very large, and the speed of the calculation will be slow [23]. In this paper, the return circuit between the train and traction substation is simulated with a π circuit, and the parameters are modified by a distributed parameter model to ensure the accuracy and speed of the simulation [24]. The simulation model is simplified without considering the effect of traction network voltage on train's traction and braking performance in this paper. In the simulation model, current of traction substation and regenerative braking train injected to the catenary is defined to be positive value and current of accelerating train and READ absorbed from the catenary is defined to be negative. The flowchart of the simulation for DC traction power system is shown in Figure 3.

Based on the simulation of the DC traction power system, the parameters of the system can be obtained, including the voltage of the catenary to rail of all nodes $\mathbf{U} = [U_1, U_2, \ldots, U_n, \ldots, U_N]$, the current of all nodes $\mathbf{I} = [I_1, I_2, \ldots, I_n, \ldots, I_N]$, and the position of all nodes $\mathbf{X} = [x_1, x_2, \ldots, x_n, \ldots, x_N]$.

For node n ($1 \leq n \leq N$), assuming that traction current of arbitrary node m ($1 \leq m \leq N$, $m \neq n$) supplying for node n is $k_{mn}I_n$, then, $\sum_{m=1,m\neq n}^{N} k_{mn} = 1$. For the analysis of rail potential at node n, the position of node n is selected as the coordinate origin, then, coordinate of the node m is transformed into $(x_m - x_n)$.

In the power supply section of node m supplying for node n, the rail current $i(x)$ and rail potential $u(x)$ of a micro element in return circuit fulfill Equation (1):

$$\begin{aligned} \mathrm{d}u(x) &= -i(x) \cdot R \cdot \mathrm{d}x \\ \mathrm{d}i(x) &= -u(x)/(R_g/\mathrm{d}x) \end{aligned} \tag{1}$$

where, R is the longitudinal resistance of the running rail, Ω/km; R_g is the longitudinal insulation resistance of the running rail to the ground, Ω·km.

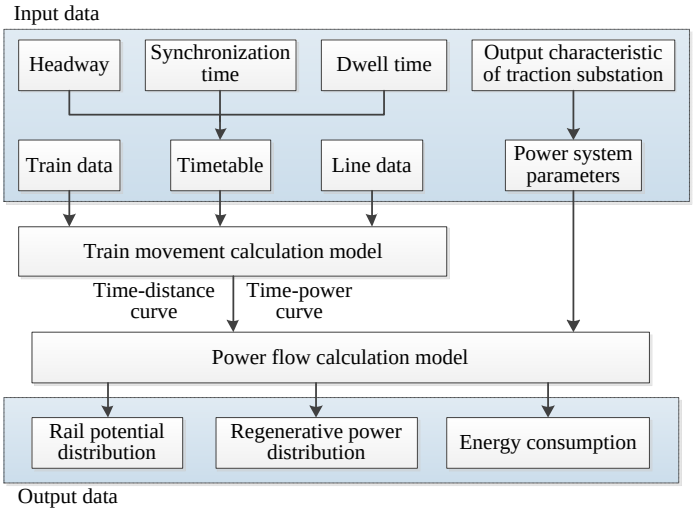

Figure 3. Flowchart of the simulation for DC traction power system.

The general solution for Equation (1) is as follows:

$$\begin{array}{c} u(x) = C_{mn1}\cosh(\alpha \cdot x) + C_{mn2}\sin\mathrm{h}(\alpha \cdot x) \\ i(x) = -(1/\sqrt{R \cdot R_g})(C_{mn1}\sinh(\alpha \cdot x) + C_{mn2}\cosh(\alpha \cdot x)) \end{array} \tag{2}$$

where, $\alpha = \sqrt{R/R_g}$, C_{mn1} and C_{mn2} are undetermined coefficients.

Traction current of node m supplying for node n is $k_{mn}I_n$, the boundary condition of rail current in the section is $i(0) = k_{mn}I_n$, $i(x_m - x_n) = k_{mn}I_n$. Based on the boundary condition and Equation (2), the undetermined coefficients can be obtained from Equation (3):

$$\begin{cases} C_{mn1} = \frac{k_{mn}I_n\sqrt{R \cdot R_g}(\cosh(\alpha \cdot (x_m - x_n)) - 1)}{\sinh(\alpha \cdot (x_m - x_n))} \\ C_{mn2} = -k_{mn}I_n\sqrt{R \cdot R_g} \end{cases} \tag{3}$$

The rail potential at node n in the power supply section of node m supplying for node n is shown in Equation (4):

$$u_{mn}(0) = C_{mn1} = \frac{k_{mn}I_n\sqrt{R \cdot R_g}(\cosh(\alpha \cdot (x_m - x_n)) - 1)}{\sinh(\alpha \cdot (x_m - x_n))} \tag{4}$$

For the parallel operation of all traction substations and trains in the line, the other nodes may supply traction current for node n. The return circuit is a linear model, the rail potential at node n can be obtained by superposing the rail potential at each power supply section as shown in Equation (5):

$$\begin{aligned} u_{ns}(0) &= \sum_{m=1,m\neq n}^{N} u_{mn}(0) \\ &= I_n\sqrt{R \cdot R_g}\sum_{m=1,m\neq n}^{N}\left[k_{mn}\left(\frac{\cosh(\alpha \cdot (x_m - x_n)) - 1}{\sinh(\alpha \cdot (x_m - x_n))}\right)\right] \end{aligned} \tag{5}$$

In Equation (5), the portion relating to the power distance for node n can be described as a function shown in Equation (6):

$$f(l) = \frac{\cosh(\alpha \cdot l) - 1}{\sinh(\alpha \cdot l)} = \coth(\alpha \cdot l) - \frac{1}{\sinh(\alpha \cdot l)} \tag{6}$$

where, l is the distance between node m and node n. Derivative of the function $f(l)$ is $f'(l) = \frac{\alpha(\cosh(\alpha \cdot l)-1)}{(\sinh(\alpha \cdot l))^2}$, and $f'(l)$ is positive when $l \neq 0$. It means that $f(l)$ is an increasing function. When the portion of traction current at node n coming from the regenerative braking train is lager, k_{mn} and $(x_m - x_n)$ is lager, and the rail potential at node n will increase. Therefore, the rail potential is influenced by the distribution of regenerative power. By optimizing the time table of multiple trains and the trigger voltage of READ, the rail potential can be controlled and the energy consumption can be reduced, in this way, maximum safety regenerative power tracking can be realized.

3. Maximum Safety Regenerative Power Tracking

In maximum safety regenerative power tracking, the train diagram and trigger voltage of READ are optimized with an improved PSO algorithm. The optimization targets are reducing the maximum absolute rail potential and energy consumption of the system. With this method, the energy consumption is reduced and the rail potential can fulfill the safety limit.

3.1. Optimization Goals

Based on the simulation model of DC traction power systems, the voltage and current of each traction substation and train can be obtained during the dynamic operation of the system. Then, the rail potential and energy consumption can be calculated. The energy consumption of the system mainly consists of network losses and energy consumption in READ. A train is the load of the system in accelerating mode which will absorb power from the catenary, and it will become a power source of the system in regenerative braking mode which will supply power for other trains or devices. Similarly, the traction substation is the power source of the line when the rectifier units work, while it will become the load of the line when READ is activated to absorb the remaining regenerative energy. The energy consumption can be calculated by the following methods shown from Equation (7) to Equation (9):

$$E_{sub} = \sum_{n=1}^{N_1} \int_{T_1}^{T_2} U_{sn} I_{sn} \mathrm{d}t, I_{sn} > 0 \tag{7}$$

$$E_{tra} = \sum_{n=1}^{N_2} \int_{T_1}^{T_2} U_{tn} I_{tn} dt \tag{8}$$

$$f_1(\mathbf{x}) = E_{loss} = E_{sub} - E_{tra} \tag{9}$$

where, U_{sn}, U_{tn} are the voltage of the catenary to running rails at the node of traction substation and train respectively. I_{sn}, I_{tn} are the current of the traction substation and train. N_1 is the total number of traction substation in the line. N_2 is the total number of train in the line. T_1 and T_2 are the start time and end time of the calculation. $\mathbf{x}$ is the parameter vector including the dwell time at each station and the trigger voltage of each READ.

Rail potential in the line can be calculated by the dynamic simulation model of DC traction power system. In the regenerative power management, the maximum absolute rail potential in the line during the operation time is another optimization goal, which can be obtained by dynamic simulation model of the system, as shown in Equation (10):

$$f_2(\mathbf{x}) = U_{rmax} = \max(|U_{rn}|), t \in [T_1, T_2] \tag{10}$$

where, U_{rn} is the rail potential at the position of node n. $\mathbf{x}$ is the parameter vector to be optimized.

3.2. Regenerative Power Management

The diagram of multiple trains and the trigger voltage of READ affect the distribution of regenerative power. For the control of maximum absolute rail potential and energy consumption, the train diagram and trigger voltage of READ are optimized in this paper.

Train diagrams will be changed by the departure interval of trains, synchronization time of the trains, dwell time at each station and running time at each power section. Departure intervals are mainly determined by the passenger flow in the line, and should not be arbitrarily adjusted. Automatic operation mode is usually adopted by trains running in the interval, and the running time in a section is fixed. In this paper, the optimization of train diagrams is mainly realized by the adjustment of the dwell time and the synchronization time of trains up-line and down-line.

A schematic diagram of the train's running time in the line is shown in Figure 4. Assuming that there are N stations in the line, the dwell time of the train down-line at each station is $t_{d1}, t_{d2}, \ldots, t_{dN}$, and the running time of the train down-line at each interval is $T_{d1}, T_{d2}, \ldots, T_{d(N-1)}$. The dwell time of the train up-line at each station is $t_{u1}, t_{u2}, \ldots, t_{uN}$, and the running time of the train up-line at each interval is $T_{u1}, T_{u2}, \ldots, T_{u(N-1)}$. The time difference of down-line train and up-line trains departing from the first station $|t_{uN} - t_{d1}|$ is the synchronization time.

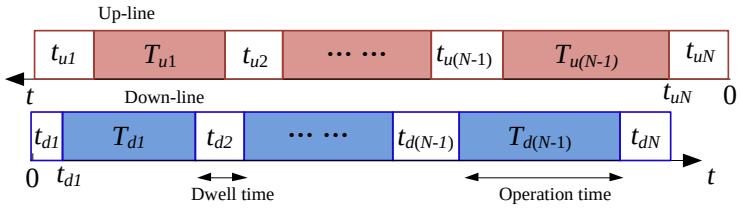

Figure 4. Schematic diagram of the train's running time.

The departure interval of trains is fixed at m seconds. Supposing that a train needs M seconds to run from the departure station to the terminal station, the maximum number of trains running in the line is $J = M/m$ (rounded up). Once the train diagram is determined, the following trains will run with the same optimized diagram. From the $(J + 1)$-th train, each m seconds demonstrate the cyclic behavior. Therefore, the simulation can be carried out during the time range $[mJ + m, mJ + 2m]$. The dwell time at each station can be adjusted, and supposing that the dwell time of j-th train at n-th station can be adjusted in the range of (a^n, b^n) seconds.

Assuming that the traction substation and READ are set at S stations of the line, the trigger voltage of the first traction substation to the S-th traction substation is U_{z1}–U_{zS}. The range of trigger voltage is between the no-load voltage U_0 and the maximum permissible voltage U_{max}.

Assuming that the dwell time of trains and the trigger voltage has k combinations, the i-th combination is shown as Equation (11):

$$\mathbf{x}_i = \{t_{d1}, t_{d2}, \ldots, t_{dN}, t_{u1}, t_{u2}, \ldots, t_{uN}, U_{z1}, U_{z2}, \ldots U_{zS}\} \tag{11}$$

In each combination of dwell time and trigger voltage, the energy consumption $f_1(\mathbf{x}_i)$ and maximum absolute rail potential $f_2(\mathbf{x}_i)$ can be obtained by the simulation model of DC traction power systems.

In this paper, the optimization goals of regenerative power management are minimizing the energy consumption of the system $f_1(\mathbf{x})$ and the maximum absolute rail potential in the line $f_2(\mathbf{x})$. The multi-objective optimization model is transferred to a single objective optimization model by ε-constraint method. Therefore, the optimization model in the paper is shown in Equation (12):

$$\begin{gathered} \min f_1(\mathbf{x}) \\ \text{s.t. } f_2(\mathbf{x}) \leq 90 \\ U_0 \leq U_{zs} \leq U_{max} \\ mJ + m \leq t \leq mJ + 2m \\ a^n \leq t_j^n \leq b^n \end{gathered} \tag{12}$$

where U_{zs} represents the trigger voltage of the READ at the n-th traction substation.

For the large number of combinations of the parameters to be optimized, an optimization algorithm is required to solve this problem. PSO algorithm has good global optimization on multi-dimensional, nonlinear, non-convex, multimodal problems. In order to solve the premature convergence in PSO, an improved PSO algorithm is applied to optimize the dwell time and trigger voltage based on simulated annealing (SA) algorithm and crossover and mutation of genetic algorithm.

In the PSO algorithm, each particle represents a possible solution to the problem. Each particle has two characteristics, the position and the velocity. In D dimension search space, the position of i-th particle is $\mathbf{x}_i$, and the speed of i-th particle is v_i. The fitness function is used to evaluate the individual in the solution. In this paper, the negative value of the energy consumption is used as the fitness function of the individual, as shown in Equation (13):

$$F[f_1(\mathbf{x})] = -f_1(\mathbf{x}) \tag{13}$$

In each iteration, update of the particle is achieved by tracking the two extrema, one is the best position achieved by the i-th individual particle $pbest_i$, and another is the best position sought by the whole particle swarm $gbest$. The $gbest$ in the last iteration is the optimal solution of the problem. The position and the velocity of i-th particle at $(k+1)$-th iteration should be updated from the k-th iteration based on Equations (14) and (15):

$$\mathbf{v}_i(k+1) = \omega \mathbf{v}_i(k) + c_1 r_1 (pbest_i(k) - \mathbf{x}_i(k)) + c_2 r_2 (gbest(k) - \mathbf{x}_i(k)) \tag{14}$$

$$\mathbf{x}_i(k+1) = \mathbf{x}_i(k) + \mathbf{v}_i(k+1) \tag{15}$$

where, ω is inertia weight. c_1, c_2 are called acceleration factor or learning factor, which is set to maintain the balance of global and local search capabilities. r_1 and r_2 are independent numbers with the range of (0, 1).

The process of the PSO algorithm is simple and the solution speed is fast. However, the algorithm easily falls into local optimal solutions. In the genetic algorithm, the crossover operation can produce a new outstanding individual, and the mutation operation can maintain the diversity of the population. In this paper, crossover and mutation are used to produce the particle with better diversity.

(1) Crossover

In the iteration of the improved PSO algorithm, a certain number of particles are selected. By exchanging the element in selected particles, a new outstanding individual can be produced. The crossover method of j-th gene in k-th particle and l-th particle is shown in Equation (16):

$$\begin{aligned} \mathbf{x}_{kj} &= \mathbf{x}_{kj}(1-b) + \mathbf{x}_{lj} b \\ \mathbf{x}_{lj} &= \mathbf{x}_{lj}(1-b) + \mathbf{x}_{kj} b \end{aligned} \tag{16}$$

where, b is a random number with the range of (0, 1).

(2) Mutation

In the improved PSO algorithm, the particle is selected with a small probability p_m, and one or more elements of the individual are changed to produce a better individual. The mutations operation of the j-th element in the i-th individual $\boldsymbol{x}_{ij}$ is shown as Equations (17) and (18):

$$\mathbf{x}_{ij} = \begin{cases} \mathbf{x}_{ij} + (\mathbf{x}_{ij} - x_{max}) \cdot f(k), r \geq 0.5 \\ \mathbf{x}_{ij} + (x_{min} - \mathbf{x}_{ij}) \cdot f(k), r < 0.5 \end{cases} \tag{17}$$

$$f(k) = r_2 (1 - k/K)^2 \tag{18}$$

where x_{max} is the maximum value of $\mathbf{x}_{ij}$. x_{min} is the minimum value of $\mathbf{x}_{ij}$. r, r_2 is the random number with the range of (0, 1). k is the current iteration number, and K is the maximum iteration number.

The SA algorithm is a computational stochastic technique for obtaining near global optimum solutions to combinatorial and function optimization problems. In this paper, SA is used in the improved PSO algorithm. In the selection of particles for crossover, the process are shown as follows:

Step 1: Initializing the first group $\mathbf{x}_1(0), \ldots, \mathbf{x}_i(0), \ldots, \mathbf{x}_N(0)$, and calculating the fitness value of each particle $F_1^0, \ldots, F_i^0, \ldots, F_N^0$.

Step 2: Calculating the initial temperature as Equation (19):

$$T_0 = 1/(F_{max} - F_{min}) \tag{19}$$

where, F_{max}, F_{min} respectively represents the maximum fitness value and the minimum fitness value.

Step 3: Calculating the ratio of crossover operation based on Equation (20):

$$P = \lambda\,(1 - k/K) \tag{20}$$

where, λ is the scale coefficient with the range of (0, 1), k is the current iteration step and K is the maximum iteration step.

Step 4: Sorting the $\mathbf{x}_1(k), \ldots, \mathbf{x}_i(k), \ldots, \mathbf{x}_N(k)$ from small to large based on the fitness value of each particle, $\widetilde{\mathbf{x}}_1(k), \ldots, \widetilde{\mathbf{x}}_i(k), \ldots, \widetilde{\mathbf{x}}_N(k)$, then, the particles with crossover operation can be selected by Equation (21):

$$\begin{cases} \text{crossover, } j > (1-P)N \\ \text{without crossover, } j \le (1-P)N \text{ and } r_c > R \\ \text{crossover, } j \le (1-P)N \text{ and } r_c \le R \end{cases} \tag{21}$$

$$R = \exp\left(-1/(T_k \Delta F_j)\right) \tag{22}$$

where, r_c is a random number with the range of (0, 1). ΔF_j is the difference between the fitness value of j-th particle and the fitness value of the global optimum.

Step 5: Cooling as shown in Equation (23):

$$T_{k+1} = \mu T_k \tag{23}$$

where, μ is the cooling coefficient, which is used for controlling the speed of temperature drop.

The steps of the improved PSO algorithm used in the regenerative power management are as follows:

(a) Initializing the first swarm of particles with random positions and velocities.
(b) Each particle is put in the simulation model of DC traction power systems to obtain the energy consumption and maximum absolute rail potential.
(c) The fitness value of each particle is calculated by the fitness function. The current position and fitness value of i-th particle are stored in $pbest_i$, and the position and fitness value of best particle are stored in $gbest$.
(d) Calculating the initial temperature T_0 based on Equation (19).
(e) Updating the position and the velocity of each particle.
(f) Mutation operation is carried out based on Equation (17).
(g) Selecting the particles for crossover based on Equations (20–22).
(h) Crossover operation is carried out based on Equation (16).
(i) Updating the $pbest_i$ and $gbest$.
(j) Checking the terminal condition (the maximum iteration number). If the terminal conditions are met, outputting the results. Otherwise, the calculation will be turned to (k).
(k) Cooling is carried out based on Equation (23), and then returning to (e).

4. Simulation Results

In this paper, the first-stage project of Guangzhou Metro Line 2 is set as an example to optimize the regenerative management. There are 10 stations in the line, and five of them are equipped with traction substations. The configuration of the line is shown as Figure 5.

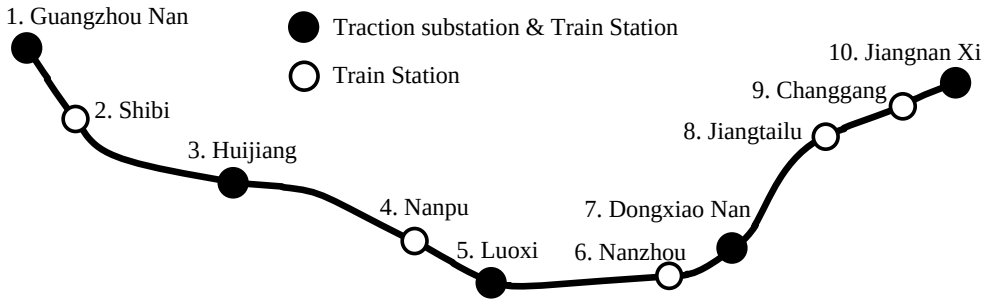

Figure 5. Configuration of the Guangzhou Metro Line 2.

The locations of the stations in the line are shown in Table 1.

Table 1. Locations of the stations.

Station Number	**1 (S_1)**	**2**	**3 (S_2)**	**4**	**5 (S_3)**
Position (m)	0	1020	3367	5800	6994
Station Number	6	7 (S_4)	8	9	10 (S_5)
Position (m)	9387	10,291	12,265	13,171	14,042

Traction substations S_1–S_5 are respectively set at the Guangzhou Nan Station, Huijiang Station, Luoxi Station, Dongxiao Nan Station, and Jiangnan Xi Staiton. The other stations are train stations.

Based on the simulation model of the DC traction power systems, the energy consumption and rail potential can be obtained during the dynamic operation of the system. The main simulation parameters are set presented in Table 2, and the whole electric data of the Guangzhou Metro Line 2 is shown in Tables A1–A4 in Appendix A.

Table 2. Main simulation parameters.

Parameter	**Value**
Internal resistance of the rectifier units R_n (Ω)	0.008
No-load voltage of the rectifier units U_0 (V)	1593
Longitudinal resistance of the catenary (Ω/km)	0.02
Longitudinal resistance of the running rails (Ω/km)	0.02
Longitudinal resistance of the buried conductor (Ω/km)	0.02
Longitudinal insulation resistance of running rail to buried conductor (Ω·km)	15
Longitudinal insulation resistance of buried conductor to ground (Ω·km)	3
Time step in the simulation (s)	1
Mismatch voltage in the iteration of power flow calculation (V)	0.01

The departure interval of the trains is 180 s, and the dwell time at each station is 30 s before optimization. The total simulation time is 3600 s. In order to analyze the rail potential and energy consumption in the period of departure process and receiving process of the trains, 11 trains depart continuously from the down-line and up-line respectively in the simulation. The end period of the simulation time is reserved for that the running time of the train may be extended in the optimization progress. The train diagram with fixed dwell time 30 s in the simulation is shown in Figure 6.

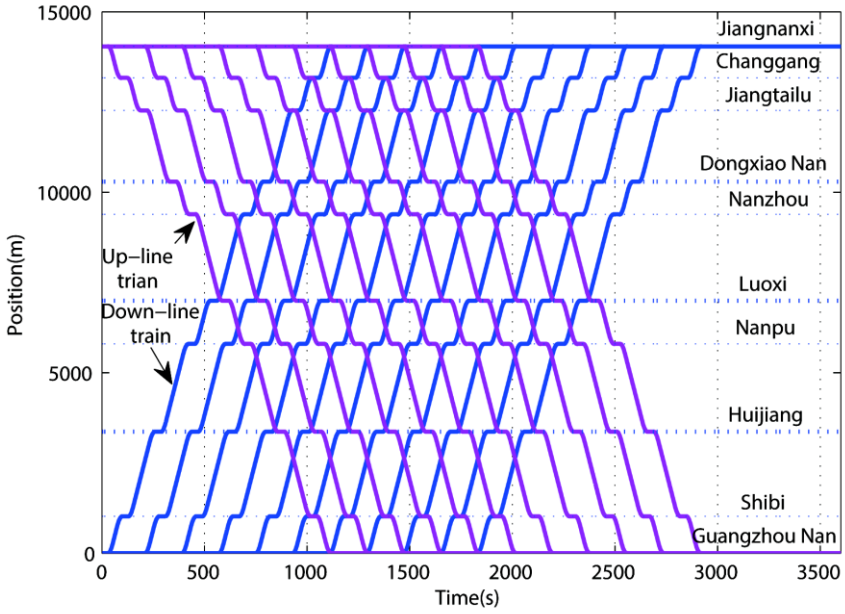

Figure 6. Train diagram with 30 s dwell time.

4.1. Effect of Regenerative Energy Distribution on Rail Potential

Simulations have been carried out on rail potential affected by regenerative power distribution. In the simulation, the dwell time at each station is 30 s, and the trigger voltage of READ is 1800 V. The rail potential distribution in the line during the dynamic operation of the system is shown in Figure 7.

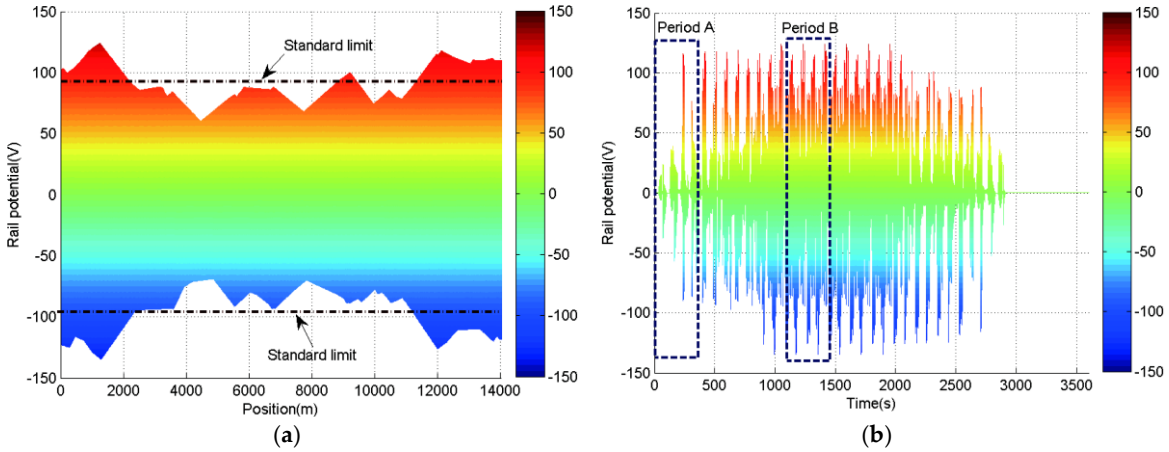

Figure 7. Rail potential distribution in the line with fixed dwell time (30 s). (**a**) Rail potential distribution in different positions; (**b**) Rail potential changes with time.

As shown in Figure 7, an abnormal rise of the rail potential exists in the line during the dynamic operation of the system. The maximum rail potential in the line is 124.12 V, and the minimum rail potential in the line is −134.58 V, which seriously exceeds the standard limit of 90 V. In order to analyze the effect of regenerative power on rail potential, period A (0–360 s) and period B (1100–1460 s) are chosen to illustrate the rail potential and power distribution as shown in Figure 8.

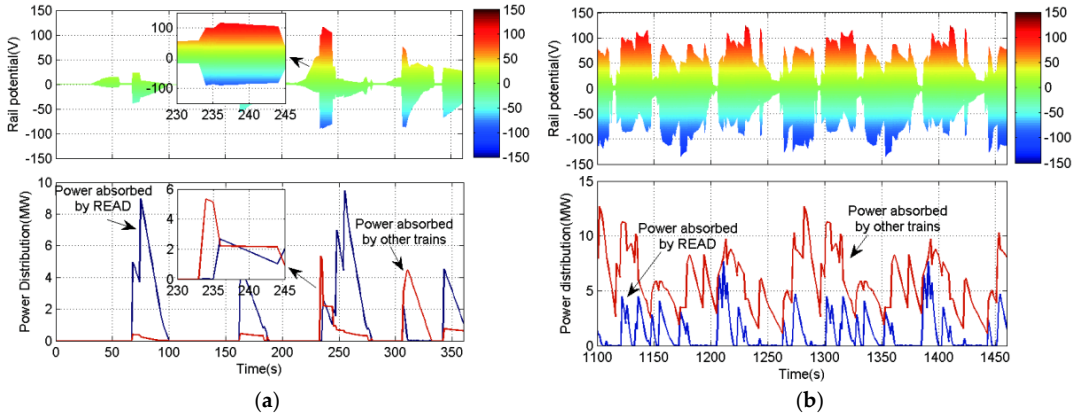

Figure 8. Rail potential and power consumption in the system with fixed dwell time (30 s). (**a**) Period A; (**b**) Period B.

As shown in Figure 8a, during the period A, the train density in the line is very low. Especially in the time from 0 s to 200 s, there are no other trains accelerating in the line when one train is in regenerative braking. The proportion of regenerative energy absorbed by other accelerating trains is low, and most of the regenerative energy is consumed in the READ. During this period, the rail potential is relatively low. When the degree of coincidence of accelerating trains and regenerative braking trains is high, such as the period from 233 s to 245 s, the regenerative power transferring over sections will increase, which can cause an abnormal rail potential rise. In this period, the rail potential can reach 115.3 V. As shown in Figure 8b, when the train density is high, the degree of coincidence of accelerating trains and regenerative braking trains is high, the regenerative energy transferring over sections increases, and the rail potential is much higher. Comparing the period of 1100–1280 s and 1280–1460 s in Figure 8b, the rail potential and power consumption of the system show a cyclical behavior after the departure process with a certain departure interval and dwell time. During the operation of the line in one day, the time of the departure process and receiving process is relative short compared with the cyclical behavior period. In the optimization, the energy consumption and maximum absolute rail potential are calculated during one cyclical behavior period (180 s). In order to analyze the effect of the regenerative power distribution on the abnormal rise of rail potential, the trigger voltages of READs in the line are adjusted synchronously to simulate the rail potential and energy consumption in the system with fixed dwell time of 30 s. The maximum absolute rail potential and energy distribution changing with trigger voltage of READ are shown in Figure 9.

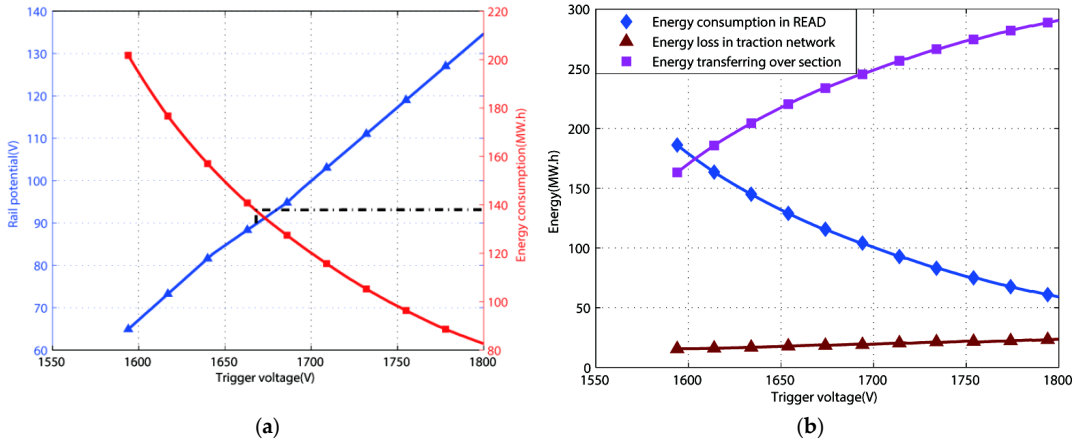

Figure 9. Changes of energy distribution with trigger voltage of READ. (**a**) Changes of rail potential and energy consumption; (**b**) Changes of energy distribution in the system.

As shown in Figure 9a, during the process where the trigger voltage of READ changes from 1800 V to 1593 V, the maximum absolute rail potential is reduced gradually, from 124.1 V to 60.89 V. In this process, the energy consumption increases gradually from 83 MW·h to 202 MW·h. When the trigger voltage of all READs is 1668 V, the maximum absolute rail potential in the line is 90V, and the energy consumption of the system is 138 MW·h. As shown in Figure 9b, in the process where the trigger voltage of READ changes from 1800 V to 1593 V, the energy consumption in READ increases from 59 MW·h to 186 MW·h, the energy loss in the traction network decreases from 23.6 MW·h to 15.6 MW·h, and the energy transferring over the section to supply accelerating trains decreases from 290 MW·h to 163 MW·h. With a low READ trigger voltage, a greater proportion of the regenerative energy fed back to the catenary will be absorbed by READ rather than by the accelerating trains in other sections. In this situation, the power transferring over the section will be low, and the rail potential is low. The energy consumption will increase with a lower READ trigger voltage. In the analysis of the effect of the regenerative energy distribution on rail potential, we do a per unit normalization for the simulation results. In the per unit normalization, energy consumption and rail potential with the fixed dwell time of 30 s and fixed trigger voltage of 1800 V are chosen to be the base value. Then, the maximum absolute rail potential and energy distribution per unit value change with the trigger voltage of READ are shown in Figure 10.

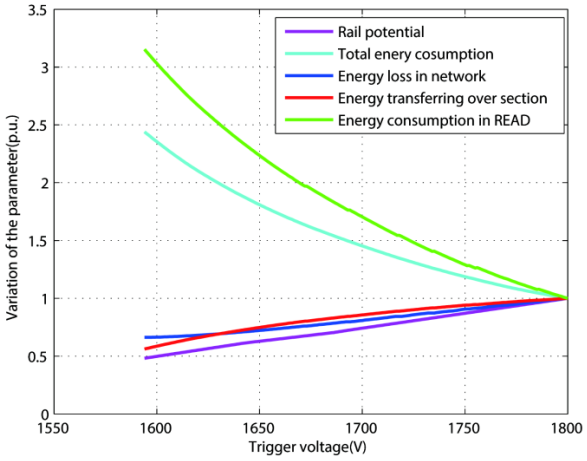

Figure 10. Variation of the parameters with per unit value.

Actually, the trigger voltage of each READ will affect the power distribution and rail potential in the line. In the optimization of regenerative power management, the trigger voltage of each READ can be adjusted. Adjustment of the train diagram can also optimize the power distribution and rail potential. In the example of this paper, if the power management is only carried out with optimization of dwell time, the maximum absolute rail potential converges to 115.2 V, which exceeds the standard limit. Therefore, the train diagram and trigger voltage should be optimized cooperatively to minimize the rail potential and energy consumption.

4.2. Control of Rail Potential Based on Regenerative Energy Management

Simulations have been carried out for maximum safety regenerative power tracking based on the PSO algorithm and improved PSO algorithm proposed in this paper. The individual size of the swarm is 40. The maximum iteration number is 120. The convergence curve of energy consumption in one cyclical behavior period (180 s) in the line during the process of optimization is shown in Figure 11.

As shown in Figure 11, by optimizing the dwell time of train and the trigger voltage of READ cooperatively based on the improved PSO algorithm, the energy consumption in 180 s converges to 98 MW·h, lower than that optimized by the PSO algorithm. Energy consumption is decreased by 29% comparing with the method where the rail potential is controlled by adjusting the trigger voltage.

After optimization, the change of the dwell time at each station after the optimization is shown in Table 3.

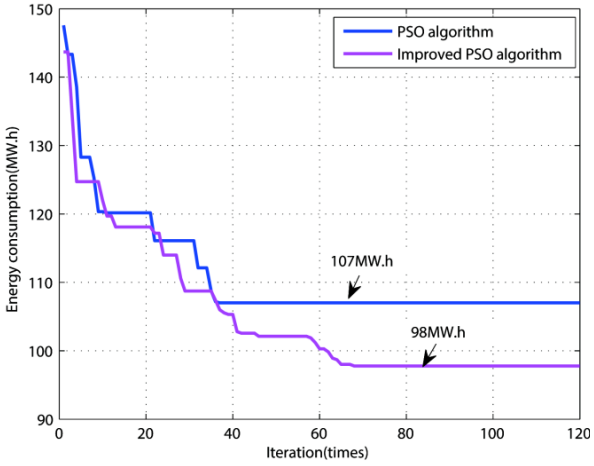

Figure 11. Convergence curve of energy consumption during the optimization.

Table 3. Change of the dwell time at each station.

Station Number	1	2	3	4	5	6	7	8	9	10
Down-line train dwell time (s)	29	34	29	33	35	29	31	26	35	29
Time difference (s)	−1	+4	−1	+3	+5	−1	+1	−4	+5	−1
Up-line train dwell time (s)	34	25	31	35	34	33	29	32	26	32
Time difference (s)	+4	−5	+1	+5	+4	+3	−1	+2	−4	+2

The trigger voltages of the READs at S_1–S_5 after optimization are 1717, 1724, 1673, 1697 and 1676 V, respectively. The total running time difference of the down-line train is +10 s, with the change rate of 0.9%. The total running time difference of the up-line train is +11 s, with a change rate of 1%. The distribution of the rail potential during the cyclic behavior period (from the time 1100 s to 1280 s) is shown in Figure 12, where the abnormal rise of rail potential can be controlled effectively by optimization of the train diagram and trigger voltage of the READ. After optimization, the maximum absolute rail potential is 86.67 V, meeting the standard limit for personal safety. The maximum absolute rail potential decreased by 35.6% comparing with the rail potential with fixed dwell time and trigger voltage.

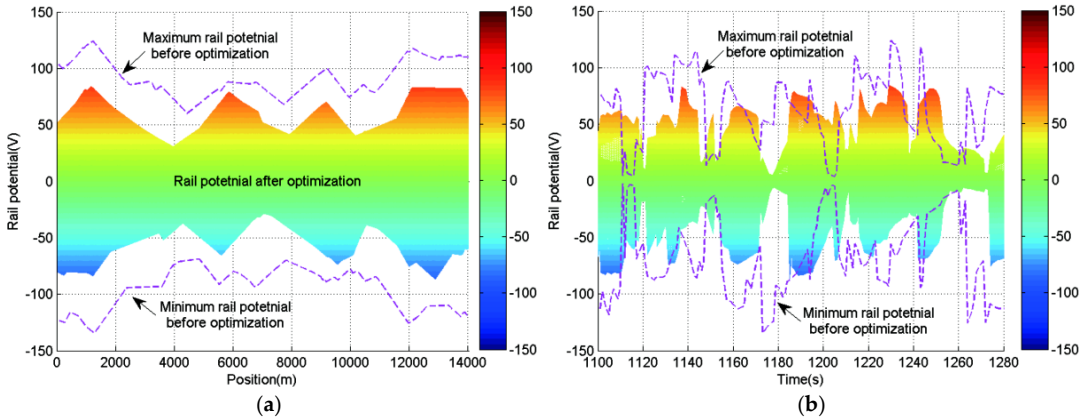

Figure 12. Rail potential distribution in the line. (**a**) Rail potential distribution in different position; (**b**) Rail potential changing with time.

The probability distribution of the rail potential before and after optimization is shown in Figure 13. As shown in Figure 13, the probability distribution of rail potential after optimization is within the range of −90–90 V, and the probability of absolute rail potential exceeding 50 V after optimization is much lower than that before the optimization.

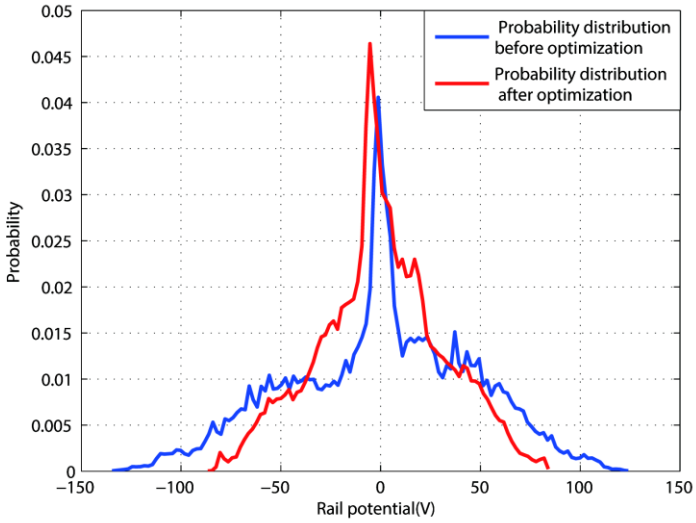

Figure 13. Probability distribution of rail potential before and after optimization.

The energy consumption of the system during one cyclic behavior period is shown in Table 4.

Table 4. Energy consumption of the system during one cyclic behavior period. p.u.: per unit.

Description	Base Case with Trigger Voltage of 1800 V and Fixed Dwell Time	Control Scheme	
		Trigger Voltage of 1668 V	Proposed in This Paper
Maximum absolute rail potential	134.58 V (1 p.u.)	90 V (0.67 p.u.)	86.67 V (0.64 p.u.)
Total energy consumption	83 MW·h (1 p.u.)	138 MW·h (1.66 p.u.)	98 MW·h (1.18 p.u.)
Energy consumption in READ	59 MW·h (1 p.u.)	119 MW·h (2.02 p.u.)	83 MW·h (1.41 p.u.)
Energy consumption in traction network	23.6 MW·h (1 p.u.)	18.6 MW·h (0.79 p.u.)	14.4 MW·h (0.61 p.u.)

As shown in Table 4, compared with the scheme where the rail potential is controlled by adjustment of the trigger voltage, the total energy consumption of the system is obviously reduced by the regenerative power management scheme proposed in this paper. The total energy consumption in a 180 s period decreases from 138 MW·h to 98 MW·h. The energy consumption in the READ decreases from 119 MW·h to 83 MW·h. The maximum absolute rail potential in the control scheme of trigger voltage set at 1668 V is 90 V, and the energy consumption in the traction network in 180 s is 186 MW·h. The maximum absolute rail potential in the scheme of regenerative energy management is 86.67 V, and the energy consumption in traction network is14.4 MW·h. The simulation results show that the control of maximum absolute rail potential based on regenerative power management can effectively decrease the energy consumption.

5. Summary and Conclusions

In this paper, maximum safety regenerative power tracking has been proposed to control the abnormal rise of rail potential and energy consumption during the operation of underground railway systems. In the optimization scheme, the train diagram and trigger voltage of READ are optimized based on the improved PSO algorithm. The management of regenerative energy can optimize the power distribution in the system, and can minimize the energy consumption under the condition that the rail potential is below 90 V. Simulation results obtained with actual data of Guangzhou Metro Line

2 show that, with the regenerative power management, the rail potential decreases from 134.58 V to 86.67 V, and the energy consumption in 180 s decreases from 138 MW·h to 98 MW·h. Maximum safety regenerative power tracking can be realized.

Acknowledgments: This work is supported by the National Natural Science Foundation of China (Grant Nos. 51147011 and E070602), and the Research and Innovation Program of Postgraduates of Jiangsu Province (KYLX 1383).

Author Contributions: Guifu Du wrote the paper and designed the simulation model; Dongliang Zhang contributed to the conception of the study and provided the line and vehicle data; Guoxin Li analyzed system model; Yihua Hu and Yang Liu helped with the optimization model. Chonglin Wang analyzed the simulation data; Jianhua Liu helped to perform the analysis with constructive discussions.

Conflicts of Interest: The authors declare no conflict of interest.

Nomenclature

a^n	Minimum dwell time at n-th station
b^n	Maximum dwell time at n-th station
c_1, c_2	Acceleration factor in PSO algorithm
C_{mn1}, C_{mn2}	Undetermined coefficients in the power supply section of node m supplying for node n
$f_1(\boldsymbol{x})$	Energy consumption of the system with parameter vector $\boldsymbol{x}$
$f_2(\boldsymbol{x})$	Maximum absolute rail potential in the line with parameter vector $\boldsymbol{x}$
F_i^0	Fitness value of i-th particle in the first group
F_{max}	Maximum fitness value in the group
F_{min}	Minimum fitness value in the group
$gbest(k)$	Best position sought by the whole particle swarm at k-th iteration
I_{sn}	Current of the n-th traction substation
I_{tn}	Current of the n-th train
k	Iteration number in PSO algorithm
k_{mn}	Ratio of the traction current that arbitrary node m supplying for node n
K	Maximum iteration number in PSO algorithm
N_1	Total number of traction substation in the line
N_2	Total number of train in the line
$pbest_i(k)$	Best position achieved by the i-th individual particle at k-th iteration
P	Ratio of crossover operation
P_{ab}	Regenerative power absorbed by READ
P_{loss}	Regenerative power consumed in the network
P_n	Power of the source or load at node n
P_{os}	Regenerative power transferring over section
P_{reg}	Regenerative power fed back to the catenary by braking trains
P_{sub}	Power supplied by traction substation
r_1, r_2	Independent numbers with the range of (0, 1)
r_c	Random number with the range of (0, 1)
R	Longitudinal resistance of the running rail
R_g	Longitudinal insulation resistance of running rail to the ground
t	Time of the simulation
t_{dn}	Dwell time of train in down-line at station n
t_j^n	Dwell time of the j-th train at n-th station
t_{un}	Dwell time of train in up-line at n-th station
T_1, T_2	The start time and end time of the calculation
T_{dn}	Running time of train in down-line at interval from n-th station to (n + 1)-th station
T_k	Temperature at k-th iteration in the improved PSO algorithm
T_{un}	Running time of train in up-line at interval from n to n + 1
$u_{mn}(0)$	Rail potential at node n in the power supply section of node m supplying for node n
$u_{ns}(0)$	Rail potential at node n

U_{dn}	Voltage of down-line catenary to earth at node n
U_{rmax}	Maximum absolute rail potential in the line
U_{rn}	Rail potential at the position of node n
U_{sn}	Voltage of catenary to running rails at the node of n-th traction substation
U_{tn}	Voltage of catenary to running rails at the node of n-th train
U_{un}	Voltage of up-line catenary to earth at node n
U_{zn}	Trigger voltage of READ at the n-th traction substation
$\boldsymbol{v}_i(k)$	Speed of i-th particle at k-th iteration
$\boldsymbol{x}$	Parameter vector including dwell time and trigger voltage
$\boldsymbol{x}_i(k)$	i-th combination of dwell time and the trigger voltage at k-th iteration
$\boldsymbol{x}_{kj}$	j-th gene in k-th particle
y_{cn}	Equivalent resistance of the traction substation n
y_{gn}	Equivalent conductance of rail to buried conductor between node n to $n + 1$
y_{pn}	Equivalent conductance of buried conductor to ground between node n to $n + 1$
z_{dn}	Equivalent resistances of down-line catenary between node n to $n + 1$
z_{rn}	Equivalent resistances of rail between node n to $n + 1$
z_{sn}	Equivalent resistances of buried conductor between node n to $n + 1$
z_{un}	Equivalent resistances of up-line catenary between node n to $n + 1$
ω	Inertia weight in the update of the optimization
λ	Scale coefficient with the range of (0, 1)
μ	Cooling coefficient
ΔF_j	Difference between the fitness value of j-th particle and the global optimum

Appendix A

The whole electric data of the Guangzhou Metro Line 2 is given below.

Table A1. Vehicle parameters.

Parameter	Value
Number of car unit N	6-car unit (4M2T)
Weights M (t)	310 (AW2)
Number of axles n	24
Max speed v (km/h)	80
Rated voltage (V)	1500
Width of the car W (m)	2.8
Height of the car H (m)	3.8
Tractive effort T (kN)	$T = \begin{cases} 350, & 0 < v < 40 \text{ km/h} \\ -4.17v + 516.7, & 40 \text{ km/h} < v < 80 \text{ km/h} \end{cases}$
Train resistance(Conventional Davis Formula) R (kN)	$R = 6.4 \times M + 130 \times n + 0.14 \times M \times v + [0.046 + 0.0065 \times (N-1)] \times W \times H \times v^2$
Braking effort B (kN)	250

Table A2. Traction substation parameters.

Parameter	Value
Capacity of the rectifier unit (kVA)	2250
Crossing impedance of the rectifier transformer	8%
Semi-crossing impedance of the rectifier transformer	6.5%
Rated secondary voltage of the rectifier transformer (V)	1180
No-load voltage of the rectifier units U_0 (V)	1593
Maxmum voltage of catenary to running rails U_{max} (V)	1800
Internal resistance of the rectifier units R_n (Ω)	0.008

Table A3. Electric network parameters.

Parameter	Value
Longitudinal resistance of the catenary (Ω/km)	0.02
Longitudinal resistance of the running rails (Ω/km)	0.02
Longitudinal resistance of the buried conductor (Ω/km)	0.02
Longitudinal insulation resistance of running rail to buried conductor (Ω·km)	15
Longitudinal insulation resistance of buried conductor to ground (Ω·km)	3

Table A4. Route parameters of the Guangzhou Metro Line 2.

Station Number	Guangzhou Nan (S_1)	Shibi	Huijiang (S_2)	Nanpu	Luoxi (S_3)
Position (m)	0	1020	3367	5800	6994
Station Number	Nanzhou	DongxiaoNan (S_4)	Jiangtailu	Changgang	Jiangnan Xi (S_5)
Position (m)	9387	10,291	12,265	13,171	14,042

References

1. Tzeng, Y.; Lee, C. Analysis of rail potential and stray currents in a direct-current transit system. *IEEE Trans. Power Deliv.* **2010**, *25*, 1516–1525. [CrossRef]
2. Chien-Hsing, L. Evaluation of the maximum potential rise in Taipei rail transit systems. *IEEE Trans. Power Deliv.* **2005**, *20*, 1379–1384.
3. Ogunsola, A.; Mariscotti, A.; Sandrolini, L. Estimation of stray current from a DC-electrified railway and impressed potential on a buried pipe. *IEEE Trans. Power Deliv.* **2012**, *27*, 2238–2246. [CrossRef]
4. Railway Applications-Fixed Installations-Electrical Safety, Earthing and the Return Circuit-Part 2: Provisions against the Effects of Stray Currents Caused by D.C. Traction Systems. Available online: http://standards.globalspec.com/std/1316409/ds-en-50122-2 (accessed on 26 June 2016).
5. Sanchez-Sutil, F.; Hernández, J.C.; Tobajas, C. Overview of electrical protection requirements for integration of a smart DC node with bidirectional electric vehicle charging stations into existing AC and DC railway grids. *Electr. Power Syst. Res.* **2015**, *122*, 104–118. [CrossRef]
6. Hernandez, J.C.; Sutil, F.S.; Vidal, P.G. Protection of a multiterminal DC compact node feeding electric vehicles on electric railway systems, secondary distribution networks, and PV systems. *Turk. J. Electr. Eng. Comput. Sci.* **2016**, *24*, 3123–3143. [CrossRef]
7. Railway Applications-Fixed Installations-Electrical Safety, Earthing and the Return Circuit-Part 1: Protective Provisions against Electric Shock. Available online: http://standards.globalspec.com/std/9987312/cenelec-en-50122-1 (accessed on 28 June 2016).
8. Ministry of Housing and Urban-Rural Construction of the People's Republic of China. *GB 50490 Technical Code of Urban Rail Transit*; Standards Press of China: Beijing, China, 2009.
9. Xu, S.; Li, W.; Wang, Y. Effects of vehicle running mode on rail potential and stray current in DC mass transit systems. *IEEE Trans. Veh. Technol.* **2013**, *62*, 3569–3580.
10. Du, G.; Wang, C.; Liu, J.; Li, G.; Zhang, D. Effect of over zone feeding on rail potential and stray current in DC mass transit system. *Math. Probl. Eng.* **2016**, *2016*, 6304726. [CrossRef]
11. Du, G.; Zhang, D.; Li, G.; Wang, C.; Liu, J. Evaluation of rail potential based on power distribution in DC traction power systems. *Energies* **2016**, *9*, 729. [CrossRef]
12. Lee, C.H.; Lu, C.J. Assessment of grounding schemes on rail potential and stray currents in a DC transit system. *IEEE Trans. Power Deliv.* **2006**, *21*, 1941–1947. [CrossRef]
13. Charalambous, C.A.; Aylott, P. Dynamic stray current evaluations on cut-and-cover sections of DC metro systems. *IEEE Trans. Veh. Technol.* **2014**, *63*, 3503–3538. [CrossRef]
14. Charalambous, C.A.; Cotton, I.; Aylott, P. Modeling for preliminary stray current design assessments: The effect of crosstrack regeneration supply. *IEEE Trans. Power Deliv.* **2013**, *28*, 1899–1908. [CrossRef]
15. Yang, X.; Li, X.; Ning, B.; Tang, T. A survey on energy-efficient train operation for urban rail transit. *IEEE Trans. Intell. Transp. Syst.* **2016**, *17*, 2–13. [CrossRef]
16. Hernandez, J.C.; Sutil, F.S. Electric vehicle charging stations feeded by renewable: PV and train regenerative braking. *IEEE Lat. Am. Trans.* **2016**, *14*, 3262–3269. [CrossRef]

17. Albrecht, T. Reducing power peaks and energy consumption in rail transit systems by simultaneous train running time control. In *Computers in Railway IX*; WIT Press: Southampton, UK, 2004; Volume 769, pp. 100–107.
18. Chen, J.F.; Lin, R.L.; Liu, Y.C. Optimization of an MRT train schedule: Reducing maximum traction power by using genetic algorithms. *IEEE Trans. Power Syst.* **2005**, *20*, 1366–1372. [CrossRef]
19. Pena-Alcaraz, M.; Fernandez, A.; Cucala, A.P.; Ramos, A.; Pecharroman, R.R. Optimal underground timetable design based on power flow for maximizing the use of regenerative-braking energy. *Proc. Inst. Mech. Eng. F J. Rail Rapid Transit* **2012**, *226*, 397–408. [CrossRef]
20. Yang, X.; Chen, A.; Li, X.; Ning, B.; Tang, T. An energy-efficient scheduling approach to improve the utilization of regenerative energy for metro systems. *Trans. Res. Part C Emerg. Technol.* **2015**, *57*, 13–29. [CrossRef]
21. Yang, X.; Li, X.; Gao, Z.; Wang, H.; Tang, T. A Cooperative scheduling model for timetable optimization in subway systems. *IEEE Trans. Intell. Trans. Syst.* **2013**, *14*, 438–447. [CrossRef]
22. Zhao, L.; Keping, L.; Shuai, S. A multi-objective timetable optimization model for subway systems. In *Proceedings of the 2013 International Conference on Electrical and Information Technologies for Rail Transportation (EITRT2013)*; Springer: Berlin/Heidelberg, Germany, 2014; Volume I.
23. Pires, C.L.; Nabeta, S.I.; Cardoso, J.R. CCG method applied to solve DC traction load flow including earthing models. *IET Electr. Power Appl.* **2007**, *1*, 193–198. [CrossRef]
24. Da Silva, J.A.P.; Cardoso, J.R.; Rossi, L.N. A fourth order differential-integral formulation applied to the simulation of the subway grounding systems. *Electr. Power Compon. Syst.* **2002**, *30*, 331–343. [CrossRef]